Contents lists available at ScienceDirect

Acta Biomaterialia

journal homepage: www.elsevier.com

Full length article

Pangolin armor: Overlapping, structure, and mechanical properties of the keratinous scales

Bin Wang,[a] Wen Yang,[a, b, *] Vincent R. Sherman,[a] Marc A. Meyers [a, c, d, *]

[a] *Materials Science and Engineering Program, University of California, San Diego, CA 92093, USA*
[b] *Department of Materials, ETH Zürich, Zürich 8093, Switzerland*
[c] *Department of Mechanical and Aerospace Engineering, University of California, San Diego, CA 92093, USA*
[d] *Department of NanoEngineering, University of California, San Diego, CA 92093, USA*

ARTICLE INFO

Article history:
Received 14 January 2016
Received in revised form 3 May 2016
Accepted 18 May 2016
Available online xxx

Keywords:
Pangolin scale
Crossed lamellae & crossed fibers
Suture-like cell membrane complex
Interlocking interface
Transverse isotropic
Strain rate sensitivity

ABSTRACT

The pangolin has a flexible dermal armor consisting of overlapping keratinous scales. Although they show potential for bioinspired flexible armor, the design principles of pangolin armor are barely known. Here we report on the overlap organization, hierarchical structure (from the nano to the mesolevel), and mechanical response of scales from ground (Chinese) and arboreal (African tree) pangolins. Both scales exhibit the same overlap organization, with each scale at the center of neighboring scales arranged in a hexagonal pattern. The scales have a cuticle of several layers of loosely attached flattened keratinized cells, while the interior structure exhibits three regions distinguished by the geometry and orientations of the keratinized cells, which form densely packed lamellae; each one corresponds to one layer of cells. Unlike most other keratinous materials, the scales show a crossed-lamellar structure (~5 μm) and crossed fibers (~50 μm). A nano-scale suture structure, observed for the first time, outlines cell membranes and leads to an interlocking interface between lamellae, thus enhancing the bonding and shear resistance. The tensile response of the scales shows an elastic limit followed by a short plateau prior to failure, with Young's modulus ~1 GPa and tensile strength 60–100 MPa. The mechanical response is transversely isotropic, the result of the cross lamellar structure. The strain rate sensitivity in the range of 10^{-5}–10^{-1} s^{-1} region is found to be equal to 0.07–0.08, typical of other keratins and polymers. The mechanical response is highly dependent on the degree of hydration, a characteristic of keratins.

Statement of Significance

Although many fish and reptiles have protective scales and carapaces, mammals are characteristically fast and light. The pangolin is the only mammal possessing a flexible dermal armor for protection from predators, such as lions. Here we study the arrangement of the scales as well as their hierarchical structure from the nano to the mesolevel and correlate it to the mechanical properties. The study reveals a unique structure consisting of crossed lamellae and interlocking sutures that provide exceptional performance and in-plane isotropy.

1. Introduction

Nature offers a plethora of structures with remarkable efficiency (performance per unit mass) for tailored functionalities, which are superior to those of many current engineered materials [1,2]. The design and mechanical functions of biological (natural) materials are, therefore, the subject of the emerging field of biological materials science, the ultimate goal being the development of novel bioinspired materials [3–6]. The particular tactics of how each biological component fulfills mechanical needs depend on its mechanical properties that are structure sensitive [7]; thus, exploring the direct link between the specially organized microstructures and the mechanical functions is fundamentally indispensable and increasingly attractive to expand the current knowledge and to create new materials.

Pangolin scales are hard keratinous tissues which are among the toughest biological materials, according to the Ashby map [1]. The pangolin is the only known mammal with this distinguishing adaptation: overlapping scales covering the body as flexible dermal armor [8]. Fig. 1a shows the protective function: the pangolin, when threatened by predators (in this case, a lion), curls up into a ball with only the hard and sharp-edged scales projecting outwards, providing protection and defense. The name, pangolin, comes from the Malay word, pengguling, meaning "something that rolls up" (Oxford dictionary). In 1820 an armor coat made of pangolin scales was presented to the King George III (Fig. 1b). The pangolins are nocturnal animals and feed on ants and termites, thus obtaining the alternative name, scaly anteaters. They are found naturally in tropical regions throughout Africa and Asia. There are eight species of pangolins, which are often divided into ground pangolins that dig and remain in underground burrows, and arboreal pangolins living in hollow trees. Typical ground pangolin (Chinese pangolin) and forest pangolin (African Tree pangolin) and their scales are shown in Fig. 1c, d. The African tree pangolins have relatively long tails (about 54% of total length) to help in climbing and hanging on trees, and the scales show a much

* Corresponding authors at: Materials Science and Engineering Program, University of California, San Diego, CA 92093, USA.
Email addresses: wey005@eng.ucsd.edu (W. Yang); mameyers@eng.ucsd.edu (M.A. Meyers)

http://dx.doi.org/10.1016/j.actbio.2016.05.028
1742-7061/

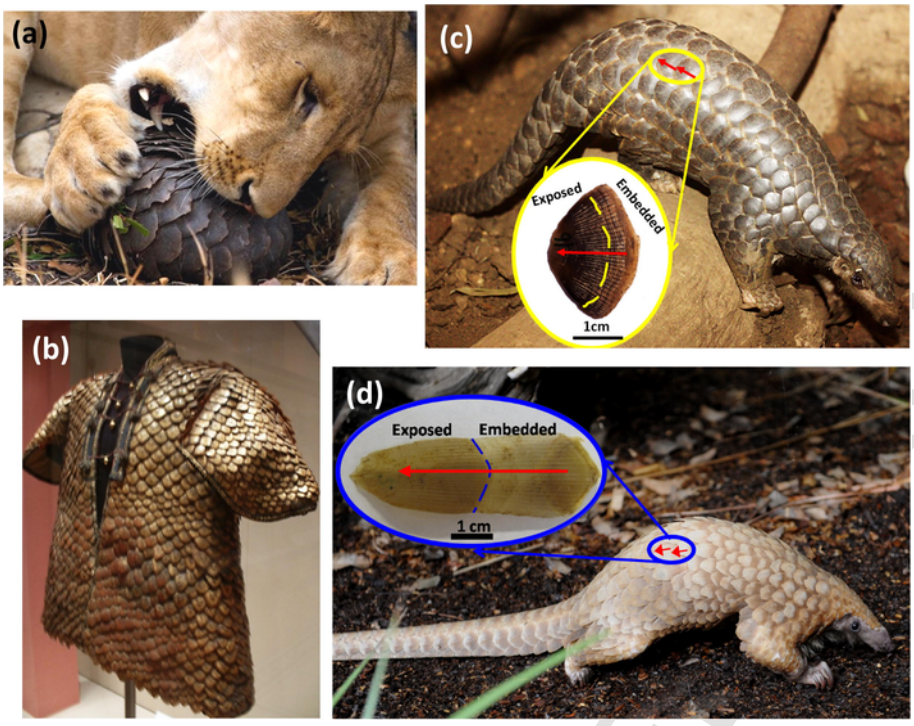

Fig. 1. (a) The protective function of the pangolin scales from the lion (predator) (http://www.animal-space.net/2010/12/lion-vs-pangolin.html); (b) an armor coat made of pangolin scales (http://commons.wikimedia.org/wiki/File:Coat_of_Pangolin_scales.JPG?uselang=zh-cn); (c) Chinese pangolin (ground type) (http://commons.wikimedia.org/wiki/File:Zoo_Leipzig_-_Tou_Feng.jpg) and the scale; (d) African Tree pangolin. Arrows indicate the scale growth direction.

higher ratio of length over width than those of the Chinese pangolin (the scale length is parallel to the scale growth direction indicated by red arrows). The scales and skin make up about 25 wt% of the pangolin's body mass [9], and the scales cover everywhere of the animal except the ventral head, ventral trunk, the inner surface of the limbs, and the foot pads [10]. Pangolin scales originate from the thick skin and continue to grow throughout the life like hair and fingernails, replacing wear loss (scale growth direction indicated by red arrows in Fig. 1b, c) [10]. The number of scales remains constant during adolescence [11].

The protective function and toughening mechanisms of the pangolin scales have not been studied in detail, since they are not as well-known as their curl-up defense [12,13]. From limited reports based on the histological structure and distribution of bound phospholipids, bound sulfhydryl groups, and disulfide bonds [13], pangolin scales can be divided into dorsal, intermediate and ventral regions through the cross section. This was suggested to be homologous with primate nails, whereas other investigators report that the pangolin scales consists of both α- and β-keratins [14], a feature of reptilian scales. Keratinous materials, e.g. wool, hoof, reveal a hierarchical structure [6]: inside the cells polymer chains assemble into intermediate filaments (IFs); then the IFs and amorphous matrix proteins may be further organized into macrofibrils and fibers for wool [15], or into fibrils and then lamellae for horns [16] and hooves [17]. In addition, the cells (keratinocytes) may encompass several macrofibrils for wool with spindle-shaped morphology (100 μm long) [18], may be arranged concentrically as lamellae (each lamella consists of one layer of cells) for horns [16] and hooves [19], or may be simply glued together for bird beaks [20]. However, corresponding information for pangolin scales is absent, and thus investigations on the protective function and toughening mechanisms are key to the understanding of biological materials.

There are few studies on the mechanical characterization on pangolin scales including abrasive properties [14,21], and hydration effect [22], since the scales need exceptional wear resistance for burrowing. In abrasion, a rotary disc drives wet abrasive sliding against scale specimens, and results from different abrasives and different sliding orientations were analyzed [14]. In dry tribological tests, the wear behavior of a steel block sliding against scale specimens under different loads and velocities was reported [21]. The water-induced recovery of mechanical properties via indentation and bending of pangolin scales was examined [22]. On the other hand, the correlation of the mechanical behavior to the nano- and micro-structures of pangolin scales remains significantly insufficient.

In an aim to understand the distinct protective function of pangolin scales, the present work investigates the overlapping mechanism, microstructure and mechanical properties. The organization of pangolin scales is compared with other scales; the morphology and the structure of pangolin scales are characterized and correlated to the mechanical behavior. Pangolin scales from both ground and arboreal types were examined. The findings and analyses presented are aimed at providing fundamental knowledge to the development of new bioinspired armor designs.

2. Materials and experimental procedures

2.1. Materials

Typical scales from ground pangolins found in southern Asia, Chinese pangolin (*Manis pentadactyla*), and from typical arboreal pangolins in central Africa, African tree pangolin (*Manis tricuspis*) were studied in this work. The Chinese pangolin scales are dark brown or yellow-brown, and have dimensions 10–30 mm wide, 20–40 mm long and 0.4–3 mm thick; the African tree pangolin scales

are russet or brownish yellow, and in average 18 mm wide, 40 mm long [11] and around 1.5 mm thick (Fig. 2). According to the shape and location on the body, two types of scales are observed: trunk scales, representative of the majority, with elongated or broad rhombic shape (Fig. 2a and b for African tree and Chinese pangolin scales, respectively), and scales at the tail edges with a folding shape at the middle of the scale with an average angle of 70–90° (Fig. 2c). The scales show longitudinal ridges on external surface (indicated by blue lines in Fig. 2a, b) parallel to scale growth direction (growth line, red arrow, Fig. 2a, b). The Chinese pangolin scales from a host with unknown age were bought from a pharmacy in China, and might have been treated by boiling water (boiling water does not significantly affect the mechanical properties, see Supplemental Fig. S1). The African tree pangolin scales were obtained from the San Diego Natural History Museum (the deceased African pangolin skin was stored in a dry container and only the internal surface of skin was preserved in a salt environment). Both kinds of scales were stored in dry containers in the laboratory with 50% relative humidity at room temperature before examination.

2.2. Structural characterization

2.2.1. Optical microscopy

The Chinese and African tree pangolin scales were cut to obtain samples with external surface (ex surf), internal surface (in surf), transverse cross section (tran-cs, perpendicular to the longitudinal ridges) and longitudinal cross section (long-cs, parallel to the longitudinal ridges) for observation. The sampling of cross sections is illustrated in Fig. 2. All samples were mounted in epoxy (Buehler, Epoxy Resin and Epoxy Hardener), ground with graded sand papers (140#, 240#, 320#, 600#, 800, 1200#, 1500#) and polished using pastes (Aluminum oxides, 0.3 μm and 0.05 μm) on a LECO VP-160 machine.

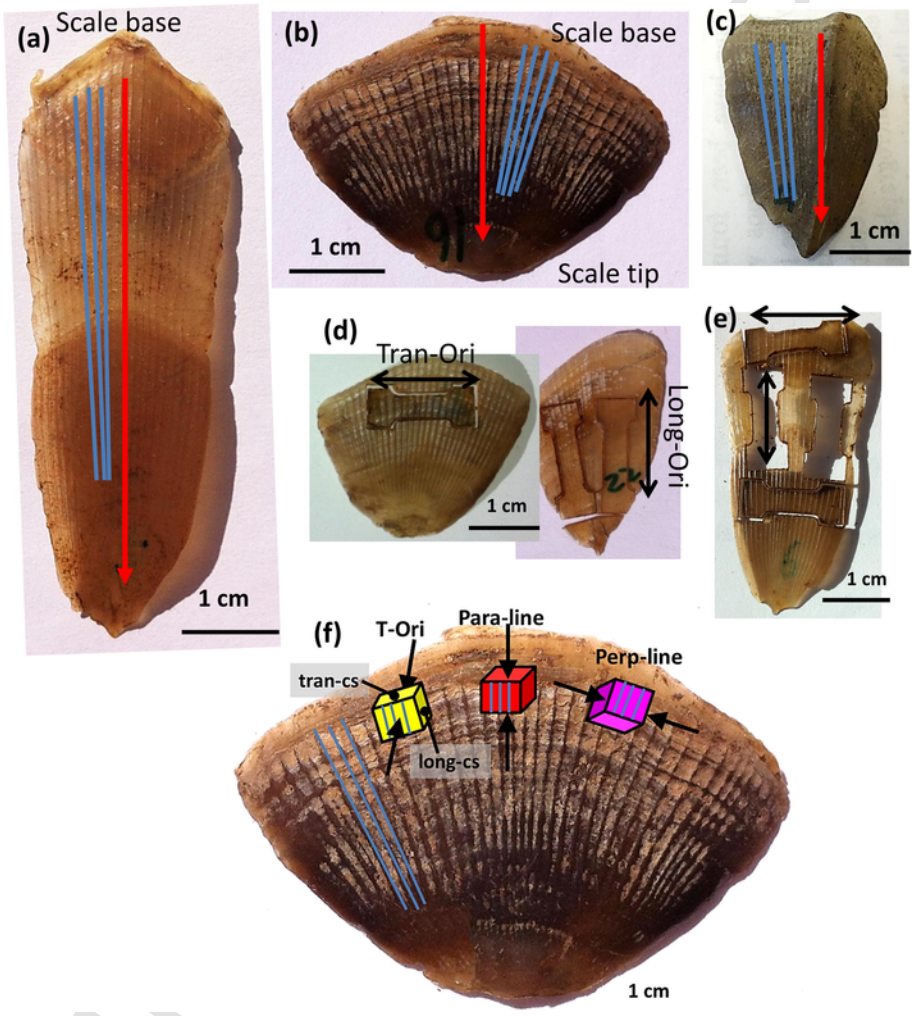

Fig. 2. Pangolin scales and sample preparation. Typical rhombic scales from (a) African pangolin and (b) Chinese pangolin, the scale growth direction from base to tip is shown (red line and arrows); the longitudinal ridges on external surface are indicated by blue lines. The longitudinal and transverse directions are parallel and perpendicular to longitudinal ridges. (c) The second type of scales with folding shape located at the tail edges of pangolin. Tensile specimens cut from (d) Chinese pangolin scales and (e) African pangolin scales in longitudinal orientation (Long-Ori) and transverse orientation (Tran-Ori). (f) Compression specimens tested in different orientations: loading through thickness orientation (T-Ori), loading along growth line direction (para-line) and loading perpendicular to growth line direction (Perp-line); blue lines represent longitudinal ridges on external surface and the transverse cross section (tran-cs); longitudinal cross section (long-cs) are shown. (For interpretation of the references to colour in this figure legend, the reader is referred to the web version of this article.)

2.2.2. Fluorescence microscopy

Scales were cut into small cubes and mounted in epoxy with tran-cs exposed and polished using the same procedure as optical microscopic observation. A fluorochrome technique involving Congo red, Titan yellow and Thioflavine T [13,23], with certain modifications was used. Cubic mounted specimens were washed in ethanol and dehydrated prior to staining. 0.02% Congo red was made and matured for 24 h, and specimens were immersed in a staining mixture of two parts of Congo red and one part of 0.1% Titan yellow for 1–2 h. The specimens were rinsed in distilled water and immersed in 0.1% Thioflavin T for 3 min. After that, they were rapidly rinsed, dehydrated through a series of graded ethanol solutions (50%, 70%, 80%, 95%, 100%, 100%, 15 min for each), and examined under ultraviolet light using an Axio Fluorescence Microscope. The keratinized cells of pangolin scales fluoresce mainly blue and the cell profiles could be readily observed.

2.2.3. Scanning electron microscopy

Scales were cut into small blocks with external and internal surfaces to examine. The tran-cs and long-cs samples were prepared via freeze fracture: scales were manually fractured after being submerged in liquid nitrogen. Then samples were fixed in 2.5% glutaraldehyde for 2.5 h, dehydrated completely in a progressive manner in graded ethanol solutions (30%, 50%, 75%, 80%, 95%, 100% twice, each for 30 min) and then placed in a critical point drying machine. All samples were coated with iridium prior to observation. Samples after tensile tests, microindentation and compression were directly coated with iridium for observation. For comparison, hair and feather rachis strips were deformed axially to fracture in tension, under conditions similar to the pangolin. The fractured segments were coated with iridium for observation. The hair was obtained from one of the authors, B. Wang, and the feathers were obtained from collected birds that died of natural causes (Federal Fish and Wildlife permit issued by US Fish and Wildlife Service). Phillips XL30 environmental scanning electron microscope equipped with energy dispersive X-ray detector and FEI XL30 Ultra High Resolution scanning electron microscope were used.

2.2.4. Transmission electron microscopy

A TGA-O_sO_4 (thioglycolic acid – osmium tetroxide) staining method [24] combined with post-staining of lead was used. Small blocks of pangolin scales (approximately 2 mm × 2 mm × 1 mm) were cut and pre-treated by immersing in 0.5 M Thioglycolic acid (pH 5.5) for 24 h at room temperature to enhance the contrast. Then the specimens were washed with double-distilled water for 1 h and immersed in 1–2% aqueous osmium tetroxide (O_sO_4) for 3 days at room temperature. Afterwards, the stained specimens were washed with distilled water, dehydrated to 100% ethanol through a series of graded alcohol solutions and then transited to 100% acetone through a graded mixture of ethanol and acetone. Then specimens were infiltrated using Spurr's low viscosity epoxy resin through a series of solutions with increasing amount of resin and decreasing amount of acetone (25% resin + 75% acetone, 50% resin + 50% acetone, 75% resin + 25% acetone, 90% resin + 10% acetone, 100% resin, 100% resin), each taking one day. Specimens were then placed in fresh resin and polymerized with appropriate orientation for 2 days at 65 °C. The embedded samples were trimmed and sectioned on a Leica Ultracut UCT ultramicrotome using a diamond knife. Silver sections were picked up and post-stained with lead for 60 s. An FEI Tecnai 12 (Spirit) (120 kV) electron microscope was used for examination.

2.3. Mechanical testing

2.3.1. Microindentation

The scales were cut into small blocks and mounted in epoxy with external surface, internal surface, transverse and longitudinal cross sections (tran-cs and long-cs) exposed. All samples were ground with graded sand papers and polished using the same sample procedure as optical microscopic observation. The well-polished samples were tested using LECO M-400-H1 (LECO, Michigan) with an applied load of 100 g holding for 15 s. Indentation measurements were performed on the external surface and internal surface along the growth line direction from scale base to tip, and on tran-cs and long-cs through scale thickness direction. Each data point reported is an average of three measurements.

2.3.2. Tensile testing

Dog-bone shape specimens were obtained using a laser cutting machine in longitudinal (Long-Ori, along the growth line) and transverse orientations (Tran-Ori, perpendicular to the growth line), shown in Fig. 2d, e. The dog-bone shape specimens had dimensions of 21 mm in length, 1.8 mm in gauge width, and the gauge length of 8 mm. The thickness varied from 0.69 to 1.29 mm for Chinese pangolin scales, and from 0.41 to 0.52 mm for African tree pangolin scales. All of the samples were cut carefully to make sure that the gauge length region was sufficiently smooth, without curvatures or extrusions from the inner surface. The side edges of the samples were polished using a dremel tool to remove the laser-heat damage while the external and internal surfaces remained untouched. An Instron 3367 equipped with 30 kN load cell was used. The tests were carried out at strain rates ranging from 10^{-5}/s to 10^{-1}/s at room temperature and relative humidity of ~50%. The average of consistent measurements of four specimens under each strain rate was reported. The fracture surfaces were coated with iridium for scanning electron microscopy.

2.3.3. Compression testing

The scales were cut and polished to achieve the compression specimens with a final dimensions of ~1.8 × 1.45 × 1.25 mm with some variation due to the natural thickness of the scales. Compressive behavior of the scales with loading in three orientations was investigated, as shown in Fig. 2f: through-thickness orientation (T-Ori) with compressive loading applied on both external and internal surfaces, parallel to the growth line direction (para-line) with the loading applied on tran-cs, and perpendicular to growth line direction (Perp-line) with loading applied on long-cs. All specimens were sampled from the embedded area of the scale, which is thicker than other parts of the scale. The tests were carried out on Instron 3367 under strain rate of 10^{-3}/s at room temperature and humidity. Average of three measurements of three specimens in each orientation was used.

3. Results and discussion

3.1. Scale overlapping mechanism

The architectural arrangement of overlapping scales shows interesting features, and the Chinese and African tree pangolin scales exhibit similar mechanism: each scale is in the center of neighboring scales arranged in a hexagonal pattern, and the internal surface partially covers three lower neighboring scales while the external surface is partially covered by three upper neighboring scales. On the internal surface, the upper rhombic region of the scale (black outline) con-

nects to the skin, while the lateral two triangular parts (blue outlines) cover the neighboring bilateral scales, and the scale tip (green outline) covers the base of a lower scale; on the external surface, the embedded area (above the yellow dotted line) is covered under three upper neighboring scales, and the lower part is exposed (Fig. 3a, d). Fig. 3b, e shows the assembly of both pangolin scales: on the internal surface of scale (i), the side portions partially cover the laterally neighboring two scales (ii) and (iii), and the scale tip partially covers the base of the lower scale (iv); on the external surface of scale (iv), the embedded area above the yellow dotted line is covered by three upper neighboring scales (ii), (i), and (iii). Fig. 3c, f shows the schematic of the overlapping pattern (dotted black, blue and green outlines represent internal surface, yellow dotted line represents external surface overlaid on the scales). This allows the scales to fully cover and protect the pangolin skin when the body moves or even curls into a ball.

The arrangement of African tree pangolin scales differs from that of Chinese pangolin scales in: (1) the shape and ratio of overlapping on the internal surface of scale; the triangles on internal surfaces in Fig. 3a and d are different, and the overlapping ratio on the internal surface (overlapped length over total length) for Chinese pangolin scale is about 30%, while for the African tree pangolin scale is about 70%; (2) the overlapping ratio on the external surface (embedded length over total length), for Chinese pangolin scale is about 19%, while that for African tree pangolin scales about 43%.

Since the African tree pangolins have scales more extensively overlapped (higher overlapping ratios on both internal and external surfaces), a point on the body is covered by three scale layers, similar to the fish scales of striped bass [25]. The difference is attributed to their different habitats and behavior. The Chinese pangolins walk on all fours very slowly, and dig burrows into the ground [26], whereas the African tree pangolins mainly live in trees, which involves more sophisticated body movements and higher degree of deformation. Their predators are also different. Therefore, the African tree pangolin covered by extensively overlapped scales minimizes the higher chances of skin exposure than the Chinese pangolin. Besides, the African tree pangolin scales have much higher aspect ratio (length over thickness, 66–85) than the Chinese pangolin scales (10–30), which results in sharper edges, as shown in Fig. 1a, and a deterrent to even lions. This also helps to reduce the number of scales needed to cover body due to the larger area of each scale, thus saving weight.

Overlapping scales can slide and shift with respect to each other, forming a flexible protective surface [27]. This has led to the historically repeated use of scale armor by warriors. Understanding the overlapping mechanism provides useful insight to the design of modern armor. Incidentally, Lorica Squamata is a flexible Roman armor

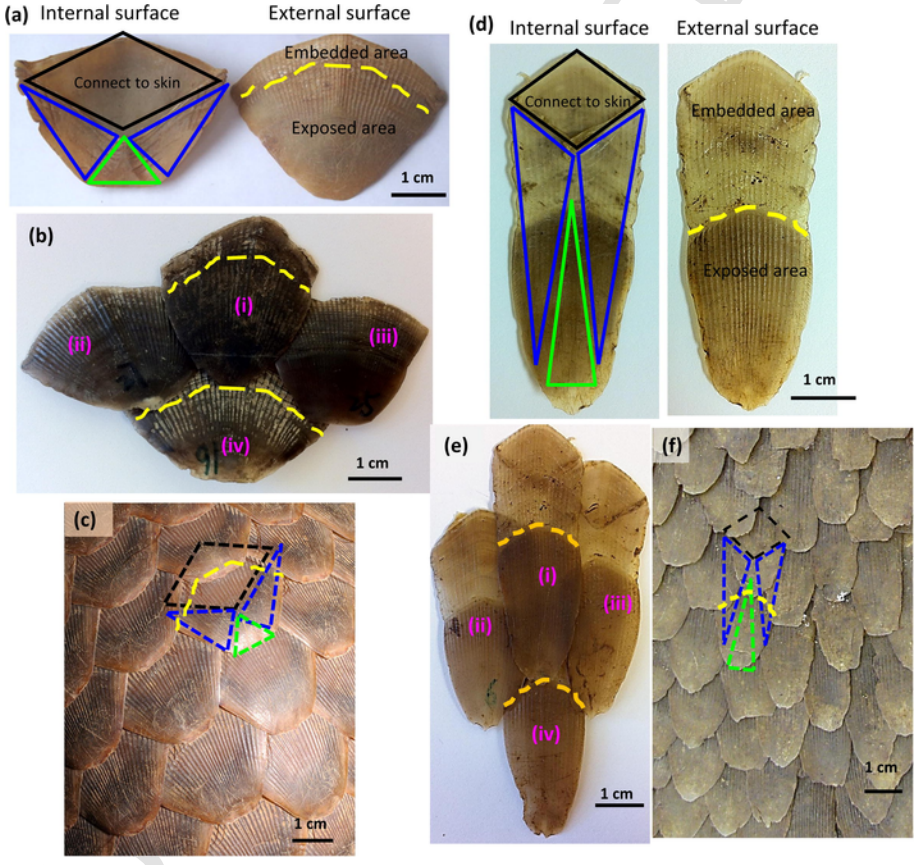

Fig. 3. Overlapping mechanism of Chinese (a-c) and African tree (d-f) pangolin scales: each scale is partially covered by three upper scales, and covers three lower scales. (a) On the internal surface, the upper rhombic area connects to the skin, the lateral parts (blue triangles) and the scale tip (green triangle) overlap with three lower scales; on the external surface, the scale base above the yellow dotted line is embedded under upper three scales, while the region below the dotted line is exposed. (b) Assembling of the scales extracted from the actual organization on pangolin: internal surface of scale (i) covers its lateral neighboring scales (ii) and (iii) and a lower scale (iv), and the external surface of scale (iv) is covered by its upper neighboring scales (ii), (iii) and (i). (c) Scales on a Chinese pangolin, with schematic drawings of overlapping mechanism from (a). (d) The internal and external surfaces of African tree pangolin scales with similar features as in (a), except different geometry and dimensions. (e) Assembling of the African tree pangolin scales, similar as that in (b). (f) Scales on an African tree pangolin, overlaid with the overlapping mechanism from (d). (For interpretation of the references to colour in this figure legend, the reader is referred to the web version of this article.)

inspired by scaled reptiles [28]. Overlapping scales are commonly seen in fish, and their scalation patterns have been well documented [29–31]. The architectural arrangement includes morphometrics of individual scales (aspect ratio and shape), inter-scale connections and joints, the degree of imbrication, and scale orientation angle [32,33].

On the one hand, pangolin scales in this work show some similarities to the overlapping structure of fish scales but exhibit different scale sizes and thicknesses. The values of aspect ratio for pangolin scales, 10–85, are in the range of fish scales, 25–100 [33], and the thickness progressively decreases towards the scale tip with thickest region around connecting to epidermis, a similar trend to fish scales [25]. Secondly, the degree of imbrication calculated as exposed length over total length of the scale measures the spatial overlap of fish scales, and varies from 0.24 to 1 for sixteen species of fish [29]. Using this definition, the degrees of imbrication of pangolin scales are about 0.81 (Chinese pangolin) and 0.57 (African tree pangolin), which also are within the range of fish scales. In addition, the scalation pattern of striped bass is reported as each scale overlapping with six other neighboring scales [25], with an imbrication degree of about 0.5, similar to the arrangement of African tree pangolin scales.

On the other hand, the overlapping of pangolin scales differs from fish scales. The pangolin scales are separated individual scales, with each one partially connected to skin; whereas, the fish scales, for instance, the striped bass, have a soft gel-like connective tissue, stratum spongiosum, between the scales [31,25], which may be an adaptation to ease scale motion in the aquatic environment.

3.2. The structure of pangolin scale

3.2.1. Morphology and cuticle structure

Both Chinese and African tree pangolin scales show, as expected, similar morphology and cuticle structure, except that the Chinese pangolin scale is shorter and wider than the African tree pangolin scale. Fig. 4a, b and e, f show that the external surfaces of both scales are convex and have longitudinal ridges with about 200 μm diameter (blue solid lines) extending from scale base to tip. Close observation of the external surfaces reveals elliptical shaped keratin scales (Fig. 5c, d, g, h) around 40–70 μm in diameter,~1 μm in thickness, and overlapped in 3–5 layers. Higher magnification of the keratin scale shows the keratin mesh morphology (Fig. 4d).

Similar keratin scales with comparable dimensions were reported briefly for porcupine quills [34] and toucan beaks [20]. Pangolin scales are keratinized materials [13], and according to the keratinization process for most keratinized materials [35], they are flattened keratinocytes that have similar dimensions to the ones on the external surface of wool [36] and stratum corneum [37,38]. For wool, the overlapping flattened cuticle cells, which differ from cortical cells in appearance, form the external cell layer, and the stratum corneum consisting of corneocytes are layers of these brick-shaped cells made of keratin mesh. Therefore, these keratin scales are the keratinized cells and different from those of the scale interior. The cuticle layer composed of flattened cuticle cells, forming a protective sheath around an inner layer of densely packed keratinized cells, is a typical structural feature of keratinous materials. It is also reported that the role of cuticular keratin cells in the bulk mechanical properties of keratin fibers is minimal, since the amorphous scales are weakly attached by the endocuticle and intercellular cement to the main fiber shaft [15].

3.2.2. Main interior structure

Both Chinese and African tree pangolin scales show three regions along the cross section, distinguished by different cell morphologies and orientations, and with different lamellar structures. From transverse cross section (tran-cs) of the scale (Fig. 5a), three regions were identified: the dorsal region (beneath the scale external surface) shows a fine structure with thin, wavy strip-like spacing (blue segments) which is parallel to the external surface, with dimensions about 20–40 μm. The ventral region (close to the scale internal surface) shows a similar fine structure which is nearly straight and paral-

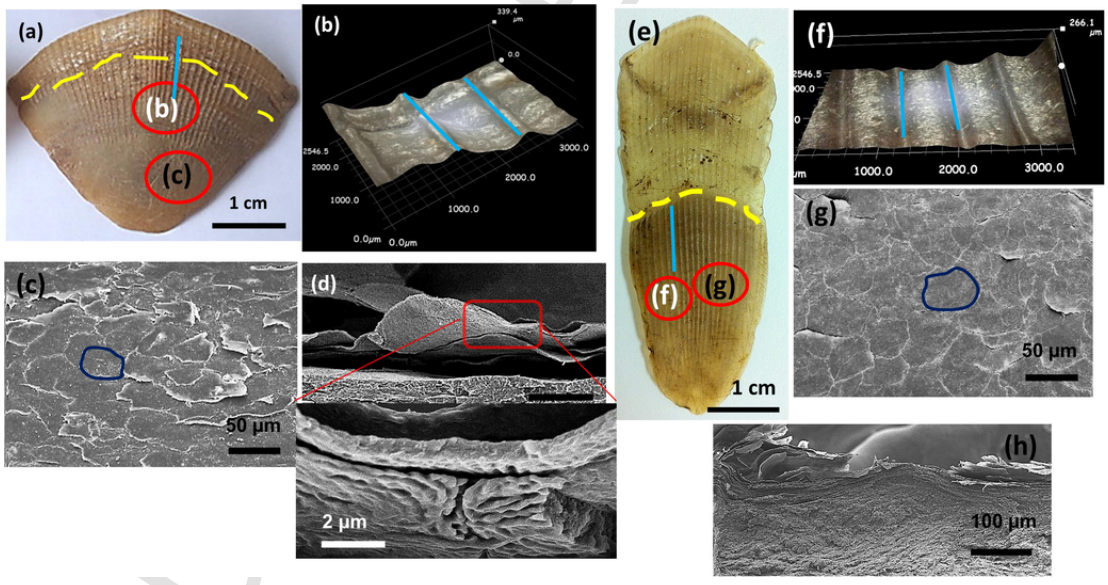

Fig. 4. Scale surface structure (yellow dotted lines indicate boundaries between embedded and exposed areas, and blue lines longitudinal ridges): (a) Chinese pangolin scale; (b) 3D optical micrograph of the scale external surface showing the longitudinal ridges parallel with growth direction; (c) plane view of the external surface showing the keratinized cuticle cells; (d) transverse cross section of the scale at the superficial 3–5 layers of cuticle cells and higher magnification image of the keratin mesh morphology; (e) African pangolin scale; (f) 3D optical micrograph of the scale external surface showing the longitudinal ridges parallel with growth direction; (g) plane view of the external surface showing the keratinized cuticle cells; (h) transverse cross section of the scale at the superficial 3–5 layers of keratinized cells. (For interpretation of the references to colour in this figure legend, the reader is referred to the web version of this article.)

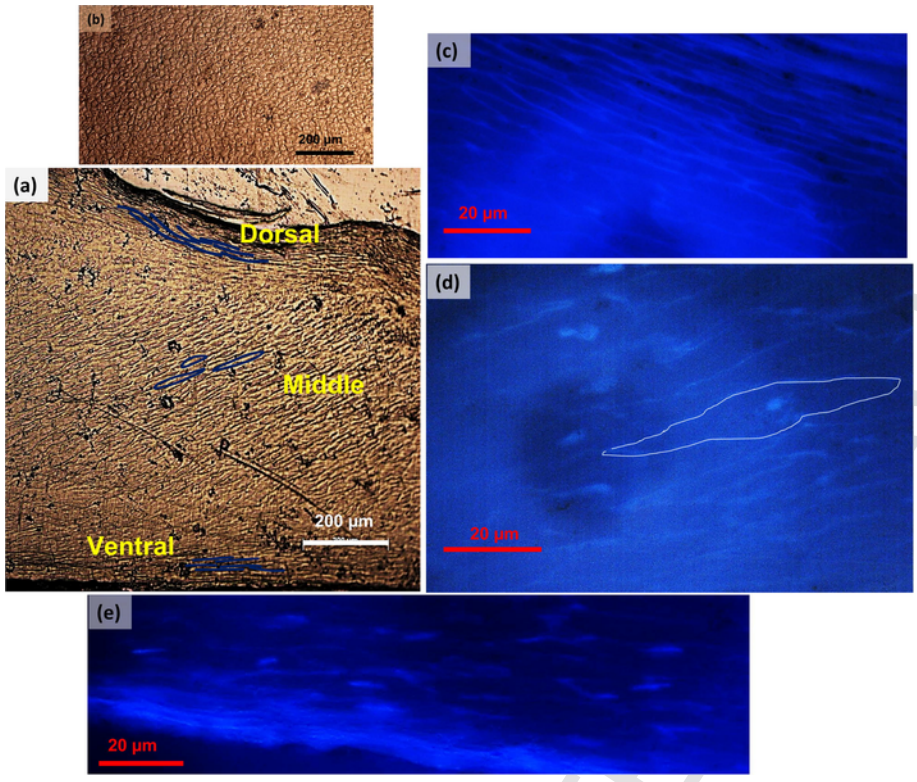

Fig. 5. Structure of scale interior: (a) optical micrograph of transverse cross section showing the dorsal, middle and ventral regions of pangolin scale; blue lines represent profiles of keratinized cells. (b) Optical micrograph of plane view of dorsal region of the scale showing the circular cell profiles. Fluorescence micrographs of (c) dorsal region showing the flattened keratinized cells, (d) middle region of tilted and less flattened cells (light-blue curves), and (e) ventral region of flattened cells parallel to scale surface. (For interpretation of the references to colour in this figure legend, the reader is referred to the web version of this article.)

lel to internal surface. The middle region, which constitutes the major part of the cross section, exhibits thicker cellular morphology tilted to the scale surface and with spacing that is larger than that of the dorsal and ventral layers. A planar view of the dorsal region of the scale in Fig. 5b (looking from the external surface) shows that the entire area exhibits homogeneous circular profiles of keratinized cells. Stained by Congo red, the keratinocytes (fluorescing blue) show clear cross sectional profiles (Fig. 5c, d, e), indicating that the spindle-shaped cells pile up to form the pangolin scale. In the dorsal region, the flattened cells are arranged in layers (around 10 cells thick) parallel to the external scale surface, with diameters about 20–50 μm and thickness 1–3 μm. The cells in the ventral region show similar morphology and arrangement as those in dorsal region, except that they are parallel to the internal surface. Keratinized cells in middle region are less flattened and usually oriented in an angle to the scale surface (tilted). They exhibit a larger size with diameter about 40–65 μm and thickness 6–10 μm. The three regions along the scale cross section agree with the reported three layers based on the histological structure and distribution of chemical constituents along cross section [13].

When fractured, pangolin scales show a lamellar structure formed by keratinized cells. Fig. 6a shows a transverse cross section (tran-cs) of a scale: the cell profiles flatten and form lamellae, and each lamella is one layer of cells. Scanning electron micrographs of transversely fractured scales also confirms the lamellar structure (Fig. 6b, c), with about 2–5 μm thickness; by comparing the morphology and dimensions of the layered keratinized cells and lamellae, one lamella is formed by one sheet of flattened cells. Scanning electron microscopic observations of both transversely and longitudinally freeze fractured scales reveal that scales show crossed-lamellae (indicated by red arrows in Fig. 6d), and exhibit three regions with different morphologies. In the dorsal region, the lamellae are well defined, and are parallel to the external surface, with one lamella around 2 μm; in the middle region, the lamellae are larger and less ordered, sometimes showing poorly defined tilted crossed-lamellae with large varying sizes (2–8 μm) and sometimes regularly tilted crossed-lamellae (2–5 μm); in the inner region, the lamellar structure is similar to that of the dorsal region: the lamellae are parallel to the scale surface, with each lamella about 1.5–3 μm thick.

The lamellar structure is widely observed in keratinous tissues, e.g. hoof wall, horn sheath, and fingernail. The bighorn sheep horn shows longitudinally aligned lamellae (2–5 μm thick), which stack along the radial direction [39]. For hoof wall, it is reported that the tubular cortex cells are organized into concentrically arranged lamellae, where each lamella is composed of one layer of cells [19], which agrees well with our observation for pangolin scales. The lamellar thickness varies from 5 to 15 μm [19]. The fingernails have been considered to be similar to pangolin scales from histological and histochemical observations [13]; they show a poorly defined lamellar structure [6,40], and also exhibit three regions along the cross section: dorsal and ventral layers of crossed-fibers or fibers without preferred orientation, and an intermediate layer of transversely aligned fibers [6,41,42].

3.2.3. Crossed lamellae and crossed fibers

When freeze-fractured (cooled in liquid nitrogen and then impacted) or loaded at a relatively high strain rate ($\sim 10^{-1}$/s), pangolin scales show a clear crossed-lamellar structure in dorsal, middle and

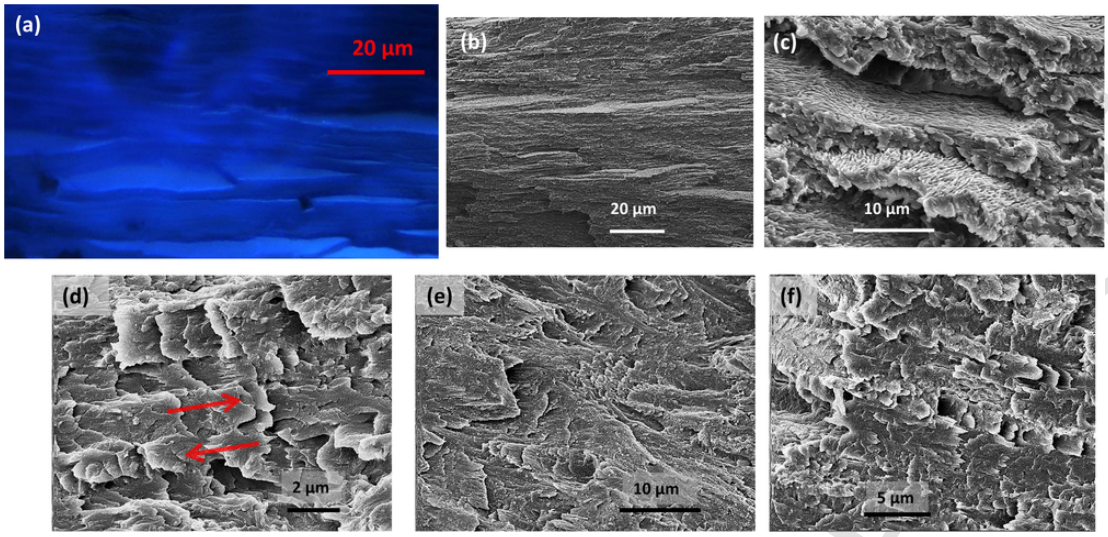

Fig. 6. The lamellar structure formed by keratinized cells: (a) fluorescence micrograph of transverse cross section (tran-cs) of a scale, the cell profiles (upper) and the lamellae are clearly seen, indicating that keratinized cells form lamellae; (b) scanning electron micrographs of tran-cs of the scale showing (a) the lamellae and (c) that each lamella is one layer of cells. Scanning electron micrographs of the three regions showing the crossed-lamellae structure: (d) dorsal region, (e) middle region, and (f) inner region.

ventral regions (Fig. 7a, b, c). These crossed lamellae occur on a spatial scale of ~5 μm. When stretched to fracture at low strain rate or in hydrated state, they show crossed fibers (Fig. 7d). These are significantly broader than the crossed lamellae, and occur on a scale of 50 μm. This is very different from other keratinous materials composed of uniaxial fibers whose fractures show fibers in one direction, e.g. human hair (Fig. 7e) and feather rachis (Fig. 7f). A tearing mode fracture was applied to pangolin scales and other keratinous materials with known fiber orientations. The pangolin scales show a zigzag profile along the torn edge, indicating that the fibers are aligned in angles to the longitudinal direction; whereas the side views of torn fractured fingernails (torn transversely along the free edge) and feather rachis (torn along the longitudinal axis) both show smooth edges, implying the majority component being uniaxial fibers (Supplemental Fig. S2).

From the above examination, it can be concluded that pangolin scales consist of crossed fibers aligned at angles to the scale growth direction. Though not usually seen in keratinous materials [6], it is an evolutionary design to achieve the protective function for pangolins. Wool and hair consist of axially oriented fibers, which is an optimized structure to resist the tensile forces from external stimuli. Nails show a dominant component of transverse fibers that direct cracks transversely rather than propagating into the delicate dermal tissue. Hoof wall and horn sheath are composed of concentrically and radially arranged lamellae with varying orientations of fibers, which provide exceptional crack diversion mechanisms to protect the inner tissue [19]. The lateral walls of feather rachis show crossed-lamellae and crossed fibers structure [6,43], which contributes to the torsional rigidity. For pangolin scales, external forces may come from biting, puncture and impact by predators and other environmental stimuli, and friction and scratch, all of which occur in unpredicted directions. A crossed-lamellar composite with fibers crossed with each other in a range of angles providing in-plane isotropy would be an optimized structure to sustain forces in diverse directions and, concomitantly, to

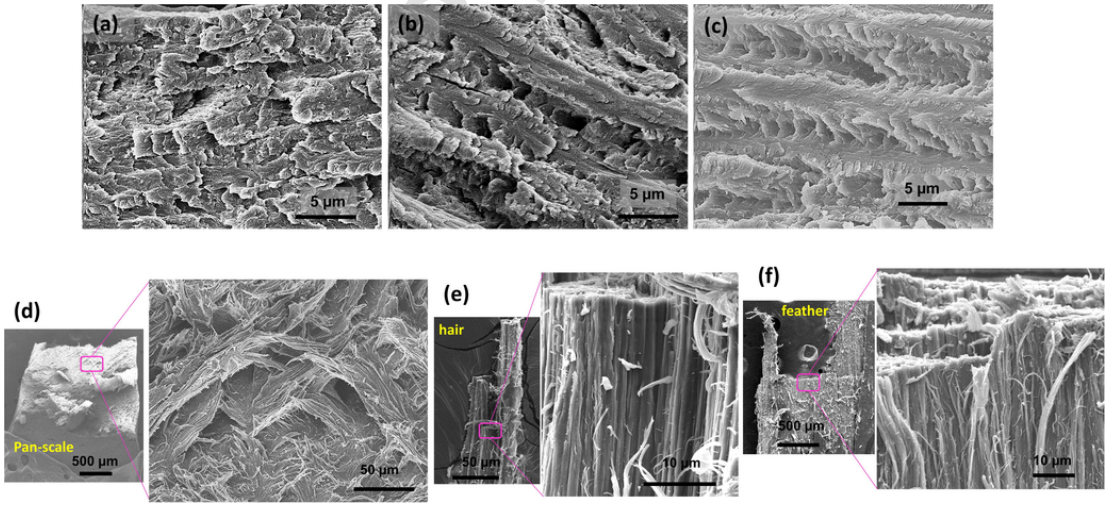

Fig. 7. Crossed-lamellar and crossed fiber structure of pangolin scales: (a) dorsal region (freeze fractured), (b) middle region (freeze fractured), and (c) ventral region (10^{-1}/s). Side views of tensile fractured specimens in three keratinized biological materials: (d) pangolin scale in hydrated state, showing crossed-fibers, (e) human hair composed of uniaxial fibers, and (f) feather rachis showing axial fibers.

increase the energy needed for crack propagation and redirecting cracks to the scale edges or tip.

3.2.4. Interlocking interface between cells and lamellae

One interesting structural feature of pangolin scales is the suture-like profile of the cell membrane complex, which creates an interlocking interface between keratinized cells and lamellae. Transmission electron micrographs of pangolin scales (plane view and transverse cross sectional specimens) show a suture-shaped structure about 25–50 nm thick: one densely stained layer enclosed by two less-dense layers (Fig. 8a), and the fine filaments with diameter about 3–5 mm (inside cells) were also observed (Fig. 8b). Considering that keratinized cells compose the pangolin scales and comparing them with the structure of wool and hair [44], this is the cell membrane complex in pangolin scales. However, unlike the cell membrane complex in wool and hair, the one in pangolin scales shows a suture-like profile, which is also captured via scanning electron micrographs (Fig. 8c, d): the suture wavelength is 250–450 nm, as observed by both transmission and scanning electron microscopy. The percentage of the interface (suture-like cell membrane complex) is calculated to be about 7.84%. The interface thickness varied from 25 to 35 nm (clearly seen in Fig. 8b). The effect of such suture-like cell membrane complex is an interlocking interface between cells and thus the lamellae, as shown in Fig. 8d.

Suture structures at macro- and micro-scales have been found in a variety of biological materials [27], e.g. turtle shell [45], seashells [46] and deer skull [47], but the cell membrane complex at the nanoscale suture structure is first reported here. The suture structure mechanically contributes to the bonding strength at the interfaces while still controlling flexibility [27]. Mechanical studies on rigid suture joints of seashells with hierarchical structures reveal enhanced load bearing capability and flaw tolerance, and prevention of catastrophic failure [46]. The suture-like cell membrane complex in pangolin scales provides increased contact area and an interlocking interface, which leads to increased bonding strength and delamination resistance between lamellae.

3.3. Mechanical behavior

3.3.1. Orientation effect on the mechanical behavior

3.3.1.1. Microindentation

Microindentation measurements in four orientations along scale growth line and scale thickness directions on both scales are shown in Fig. 9. The Chinese pangolin scales show a similar microhardness, fluctuating around 220 MPa, when indented on the external (ex surf) and internal (in surf) surfaces along scale growth line direction; this suggests the same structure from scale base to tip. The African tree pangolin scales show slightly lower microhardness values, about 200 MPa, and a similar trend indenting on external and internal surfaces along the growth line direction. Indentation on the transverse (tran-cs) and longitudinal (long-cs) sections of Chinese pangolin scales generates the same microhardness value (Fig. 9b), implying an isotropic behavior of the scale, which agrees again with the structure of crossed-fibers between lamellae. The African tree pangolin scales show similar hardness on cross sections, albeit at a consistently slight lower value (~180 MPa).

The higher harness on the surfaces in comparison with on the sections may be understood from the relative orientations of the layered keratinized cells and loading direction: indenting on surfaces along scale growth line is applying a force in the denser orientation (scale thickness direction, highest compressive strength), while indenting along scale thickness is applying load in the cell plane direction (lower compressive strength). However, one should note that this difference is not significant. After indentation, the scales show clear smooth indents, and the lamellae are deformed without observed

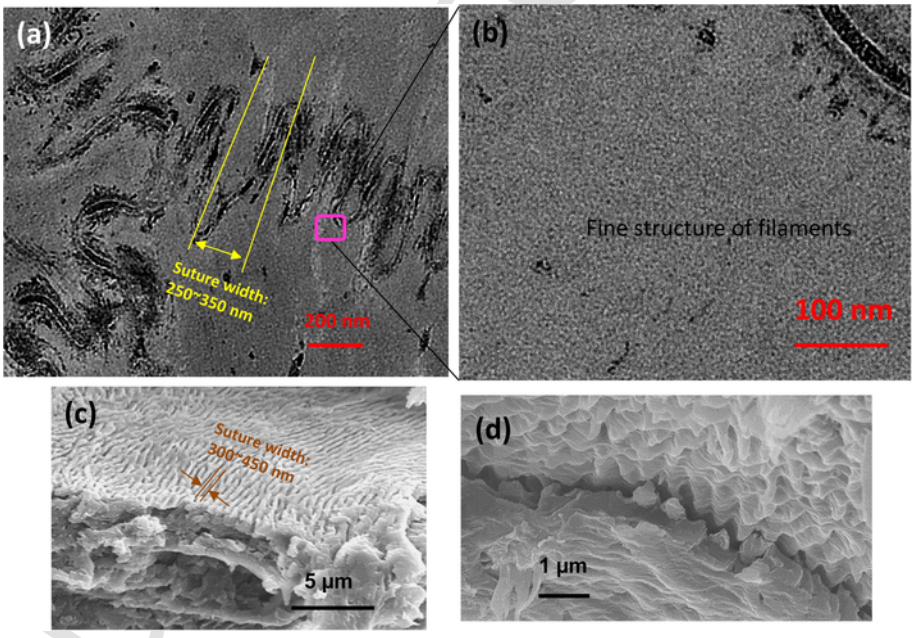

Fig. 8. The suture-like cell membrane complex and the fine filaments of pangolin scales: (a) transmission electron micrograph of transverse cross section (tran-cs) of a scale. The cell membrane complex (about 25–50 nm thick) consists of one densely-stained central layer and two less dense layers, typical of keratinous materials, but interestingly shows suture-like profile (suture width ~350 nm); (b) transmission electron micrograph of the area in (a) showing the fine filaments about 3–5 nm in diameter inside cells. Scanning electron micrographs: (c) tran-cs of the scale, the lamellae also show fine suture-like protrusions, since they are formed from flattened keratinized cells; (c) and (d) the suture-like cell membrane complex provides interlocking interface between lamellae.

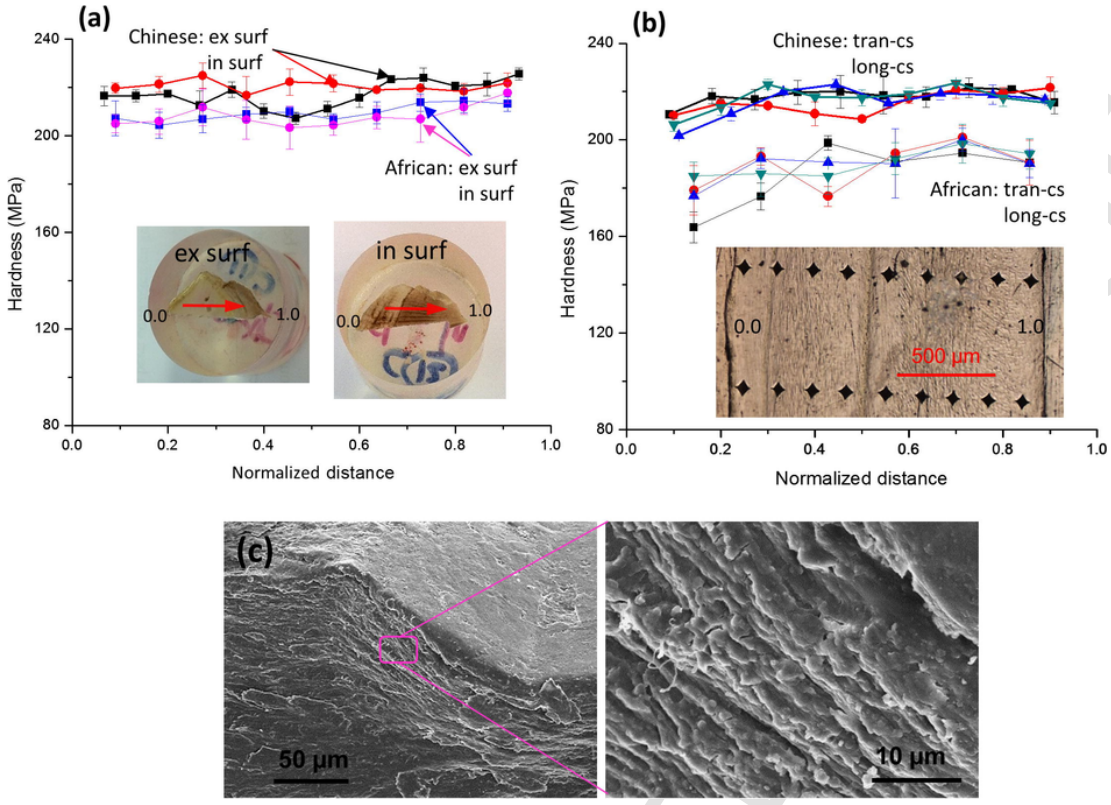

Fig. 9. Mircohardness results of the scales: (a) hardness values of African tree and Chinese pangolins scale along on external surface (ex surf) and internal surface (in surf) along growth line direction (red arrows, from scale base to tip); (b) hardness values of African tree and Chinese pangolin scales indenting on transverse (tran-cs) and longitudinal (long-cs) along thickness direction. (c) Scanning electron micrographs of the indent (flat region in c) showing the compressed lamellae. (For interpretation of the references to colour in this figure legend, the reader is referred to the web version of this article.)

cracking (Fig. 9c), which corroborates the high ductility in compressive testing.

3.3.1.2. Tensile response

The tensile behavior of African tree and Chinese pangolin scales loaded in the longitudinal and transverse orientations (Long-Ori and trans-Ori) is shown in Fig. 10a, b; the results are summarized in Table 1. Both exhibit similar stress-strain curves that show two stages: an elastic region that is fairly linear, and then a region with a gradually decreasing slope, the latter representing permanent deformation; the third stage is a negative slope, indicative of damage to the structure. This is somewhat different from the three regions (elastic, yield, post yield) shown in stress-strain curves of most typical α-keratinous materials [6], such as wool [48] and hoof wall [49], but similar to β-keratinous materials, e.g. keratin rhamphotheca of bird beak [20], feather rachis cortex [50]. Such features suggest that the pangolin scales are not solely composed of α-keratin (verified by X-ray scattering patterns, unpublished results), but a combination of α- and β-keratins, since α-keratin usually generates stress-strain curves with an initial linear region and a plateau yield region followed by a stiffened post-yield region, implying the α to β transition. In addition, the pangolin scales show crossed lamellae, and the fibers are crossed between lamellae rather than uniaxially aligned; whereas the α-keratin fibers in, e.g. wool and hagfish slime threads [6], are perfectly aligned along the axis, and therefore, the α to β transition upon axial stretching is clearly visible by a plateau.

One interesting feature is that both scales show similar tensile behavior when stretched longitudinally and transversely: the ranges of stress-strain curves in the two orientations almost overlap each other (Young's modulus around 1 GPa, and tensile strength about 70 MPa), and the fracture surfaces in the two orientations show the same crossed-lamellae structure (Fig. 10c, d). These corroborate the structural observation that pangolin scales are composed of keratinized cells forming crossed lamellae that are the same in longitudinal and transverse orientations, thus exhibiting transverse isotropic tensile behavior. The toucan rhamphotheca (β-keratin) also shows no systematic difference in modulus and yield strength along the two orientations [20]. In contrast, most α-keratinous materials show superior mechanical properties in certain orientations for specific functions discussed previously, e.g. wool, hair, and hagfish slime fibers in the axial direction, and nails along the lateral edge [6]. As mentioned earlier, this transverse-isotropic mechanical response is needed for the specific functionalities of the scale.

3.3.1.3. Compressive behavior

Compressive loads occur frequently during life of pangolin scales. Fig. 11 shows the compressive stress-strain curves of Chinese pangolin scales in three loading orientations; the results are summarized in Table 2. The compressive strength (stress at the onset of plateau region) shows highest value in the scale thickness direction (T-Ori), 127 MPa, followed by the loading parallel to the scale surface: Perpline (113 MPa) and para-line (92 MPa). This is advantageous for the scales since the most often experienced compressive force exerted predators (such as biting from lions) is perpendicular to the scale thickness plane. After a plateau region, the compressive stress rises continuously, squeezing specimens into a flattened disk without fracture, indicating good ductility and energy absorbance ability. The

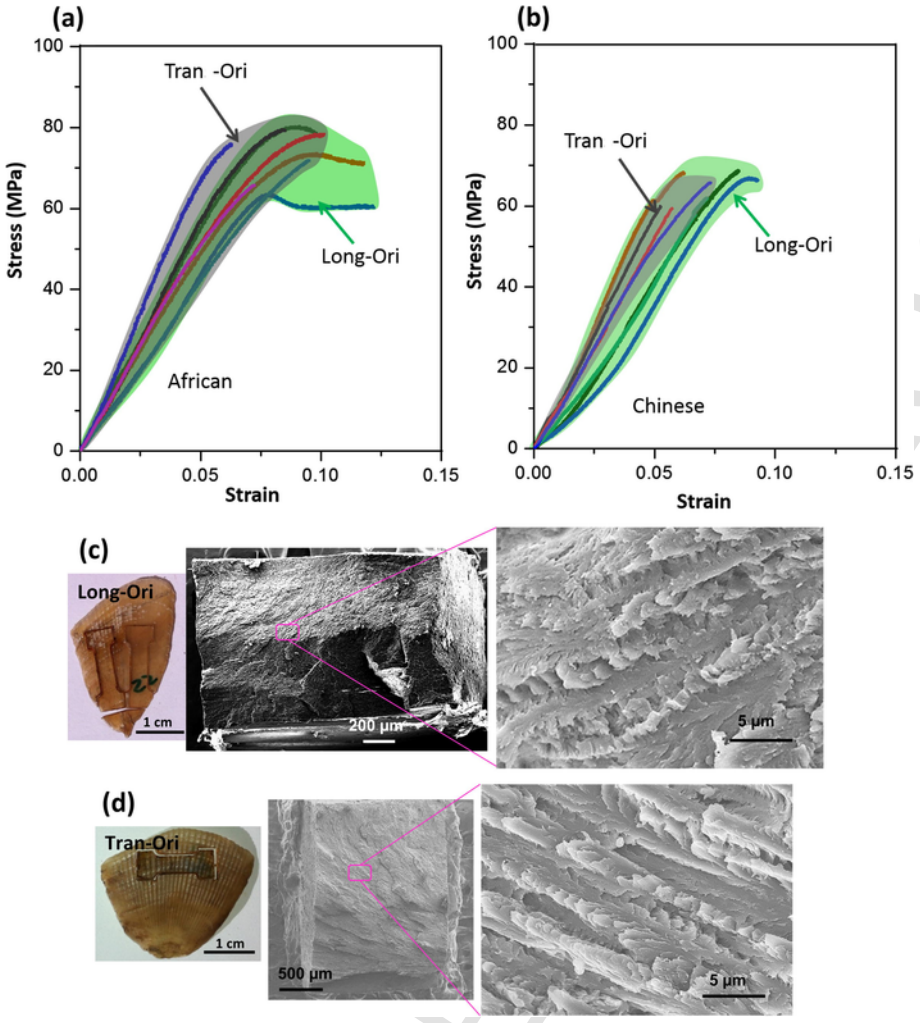

Fig. 10. Tensile response of the (a) African pangolin and (b) Chinese pangolin scales loaded in longitudinal (Long-Or) and transverse (Tran-Ori). Fracture surfaces of Chinese pangolin scales from (c) Long-Ori and (d) Tran-Ori.

elastic modulus changes little among these three orientations, around 2.2 GPa, which agrees well with structural observation.

The different compressive strengths but similar moduli among three orientations originate from the arrangement and dimensions of keratinized cells and the lamellar structure. The fibers are crossed between lamellae, thus loading in three orientations generate similar elastic moduli. In addition, the keratinized cells, which form lamellae, are flattened and pile in layers through the scale thickness direction, resulting in a denser orientation than the cell plane direction (including Perp-line and para-line orientations); therefore, loading in T-Ori leads to higher compressive strength than the other two loading directions. In the other orientations, axial splitting may occur along lamellar boundaries. The horn keratin from bighorn sheep (α-keratin) is reported to exhibit similar elastic modulus and yield strength when compressed longitudinally and transversely, but poorer properties in the radial direction, which was also attributed to the loading directions parallel or perpendicular to the lamellar orientations [39].

In brief summary, pangolin scales show transverse-isotropic properties, demonstrated from tensile, compressive and microindentation responses tested in different orientations, and slightly superior strength in the scale thickness direction than that in longitudinal and transverse orientations. This correlates with the structural design of the scales, which involves flattened keratinized cells forming lamellae and crossed fibers between lamellae. Such mechanical features are correlated with the protective functions for the pangolins, and are also requisite for body armor materials.

3.3.2. Effect of strain rate

3.3.2.1. Tensile stress-strain behavior

Fig. 12 shows the tensile behavior and strain-rate sensitivity of African tree and Chinese pangolin scales. The stress-strain curves, for all strain rates, show an elastic region followed by a region with decreasing slope and failure. For African tree pangolin scales, as the strain rate increases from 10^{-5} to 10^{-1}/s, generally the Young's modulus and tensile strength increase from 1.1 to 1.5 GPa and from 65.5 to 108.7 MPa, respectively. The breaking strain decreases somewhat from 16.8 to 11.9%, while toughness (area under stress-strain curve) does not change in a consistent manner, varying from 8.29 MJ/m^3 at 10^{-5}/s, 4.92 MJ/m^3 at 10^{-4}/s to 8.39 MJ/m^3 at 10^{-1}/s. The Chinese pangolin scales exhibit similar tensile behavior, with slightly larger scattering at each strain rate, shown in Fig. 12b. The Young's modulus and tensile strength increase, though not significantly, with the increase of strain rate: from 0.9 GPa and 60.4 MPa at 10^{-5}/s to 1.2 GPa and 74.2 MPa at 10^{-1}/s, respectively. Both breaking strain and toughness decrease with increasing strain rate. At the strain

Table 1
Tensile results of African tree and Chinese pangolin scales in longitudinal and transverse orientations (± standard deviation).

		Strain rate (/s)	Young's modulus (GPa)	Tensile strength (MPa)	Breaking strain (%)	Toughness (MPa)
African tree pangolin scale	Long-Ori	10^{-5}	1.1 ± 0.3	65.5 ± 6.7	16.8 ± 5.5	8.3 ± 3.3
		10^{-4}	1.1 ± 0.2	71.5 ± 6.6	10.6 ± 2.7	4.9 ± 1.5
		10^{-3}	1.0 ± 0.1	72.4 ± 6.9	12.9 ± 0.3	6.5 ± 0.6
		10^{-2}	1.1 ± 0.1	84.7 ± 9.8	12.6 ± 0.8	7.2 ± 0.7
		10^{-1}	1.5 ± 0.2	108. 7 ± 6.0	12.0 ± 3.6	8.4 ± 3.3
	Tran-Ori	10^{-3}	1.2 ± 0.2	74.2 ± 5.1	8.4 ± 1.4	3.6 ± 0.9
Chinese pangolin scale	Long-Ori	10^{-5}	0.9 ± 0.1	60.4 ± 9.0	11.4 ± 3.8	4.8 ± 2.9
		10^{-4}	1.0 ± 0.1	60.5 ± 6.5	12.0 ± 3.1	4.7 ± 1.8
		10^{-3}	1.0 ± 0.2	66.4 ± 2.7	8.0 ± 1.4	2.7 ± 0.5
		10^{-2}	1.0 ± 0.1	70.8 ± 10.9	8.7 ± 0.7	3.4 ± 0.4
		10^{-1}	1.2 ± 0.1	74.2 ± 2.3	6.8 ± 0.1	2.5 ± 0.1
	Tran-Ori	10^{-3}	1.1 ± 0.1	61.6 ± 2.8	6.1 ± 0.9	2.0 ± 0.5

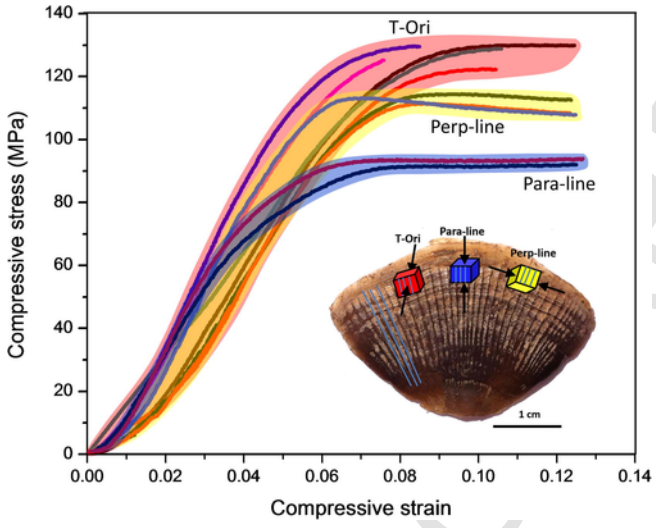

Fig. 11. Compressive stress-strain curves of Chinese pangolin scales loaded in three orientations.

Table 2
Compression results of Chinese pangolin scales in three orientations (± standard deviation).

	Elastic modulus (GPa)	Compressive strength (MPa)
Thickness orientation (T-Ori)	2.2 ± 0.3	127.3 ± 2.9
Para-line	2.2 ± 0.2	92.0 ± 0.9
Per-line	2.3 ± 0.3	112.8 ± 1.1

rate of 10^{-4}/s, both pangolin scales show certain level of necking and obvious crazing (whitening of the necking region).

As expected for a viscoelastic material, pangolin scales become stiffer and stronger with increasing loading rate; the breaking strain and toughness do not change much for African tree pangolin scales, but decrease for Chinese pangolin scales. Such strain-rate dependence provides the pangolin scales an increased ability to combat impacts or strikes with higher stiffness and strength, and to absorb more energy to delay the onset of failure when loaded slowly, a key mechanism for coping with forces from the environment. This strain rate effect is crucial to body armor for humans. As the strain rate increases, large-scale movement of the molecules in a viscoelastic material is restricted, thus leading to increased modulus and strength, but a decreased maximum strain. When loaded slowly, the chains of the polymer composite are able to deform to a larger degree and to slide past each other, allowing the scales to absorb more energy before failure.

The strain rate sensitivity of pangolin scales can be characterized by the strain rate sensitivity index, *m* [51]:

$$\sigma_y = K\dot{\epsilon}^m \tag{1}$$

where σ_y and $\dot{\epsilon}$ are the yield stress and strain rate, K is a constant. Therefore, *m* can be calculated through Eq. (2):

$$m = \frac{\partial \ln \sigma_y}{\partial \ln \dot{\epsilon}} \tag{2}$$

The yield stresses for African tree and Chinese pangolin scales were calculated from the stress-strain curves and show increased values with increasing loading rate. Fig. 12c plots the $\ln\sigma_y - \ln\dot{\epsilon}$ curves for African tree and Chinese pangolin scales; the values of *m* are 0.070 and 0.081, respectively. The variation of yield stress from 10^{-5}/s to 10^{-1}/s for African tree pangolin scales is slightly smaller than that of Chinese pangolin scales, leading to a slightly smaller calculated strain rate sensitivity. Generally, African tree and Chinese pangolin scales show similar strain rate dependent behavior, and the strain rate sensitivity index values are comparable.

Fig. 12d provides values of the strain rate sensitivity, *m,* for different materials as a comparison: common polymers, e.g. polycarbonate (*m* = 0.03), polymethyl methacrylate (*m* = 0.07) exhibit similar *m*. Yu et al. [52] report the strain-rate sensitivity for human hair equal to 0.11 (Fig. 12d).

A high strain-rate sensitivity also observed in other keratinous materials, such as wool [53] and equine hoof wall. Kasapi and Gosline [49] report an increasing Young's modulus (0.28 GPa at 10^{-3}/s to 0.85 GPa at 70/s) and yield strength with increasing strain rate for hydrated hoof wall keratin. The viscous component in wool has been considered the matrix proteins [54], while the fibrous phase (microfibrils) contribute to the initial elasticity. The bird beak rhamphotheca (β-keratin) shows a pull-out fracture mode at low strain rate (5×10^{-5}/s) and brittle fracture (keratin scales were torn) at higher strain rate (5×10^{-2}/s). The transition of fracture mode was explained in terms of the competition between viscoplastic shear of the interscale glue and tensile fracture of the scales [55]. Since pangolin scales consist of α- and β-keratins, the amorphous matrix proteins and the fibrous phase are probably the viscous and elastic components, respectively, and the bonding between keratinized cells/lamellae plays a role in determining mechanical properties.

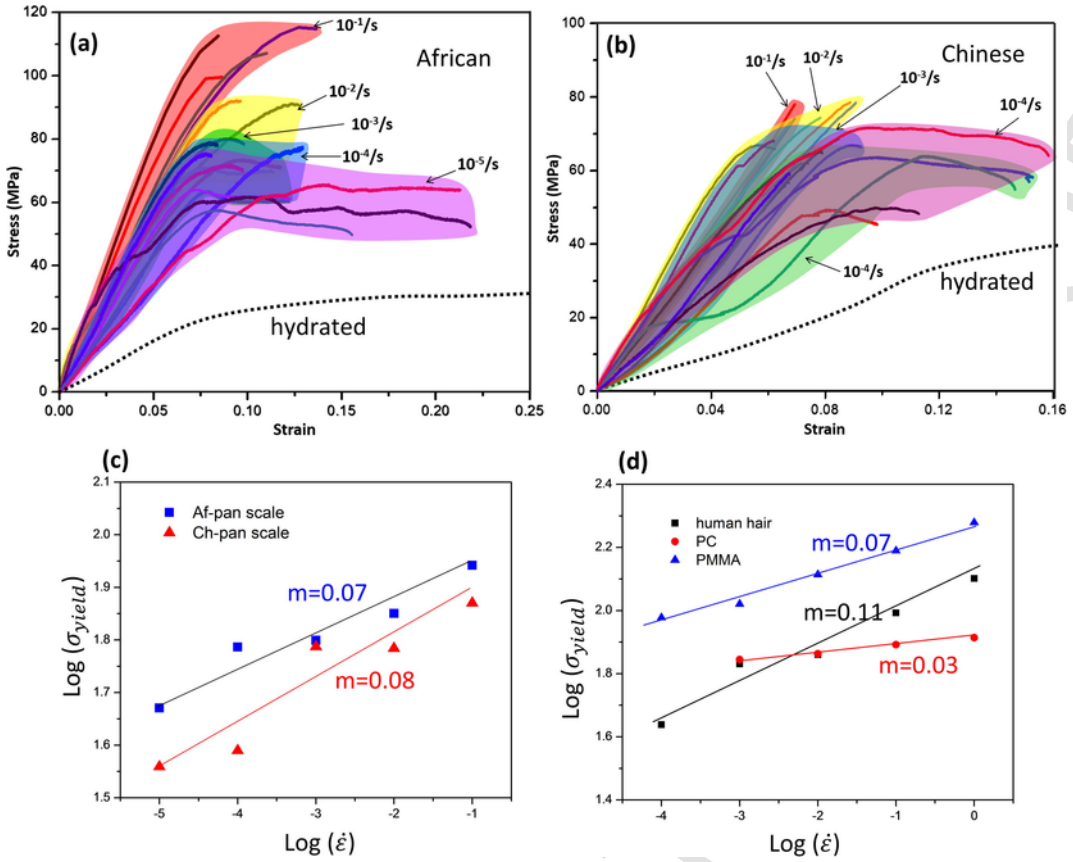

Fig. 12. Strain rate and hydration sensitivity of pangolin keratin: (a) tensile stress-strain curves of African tree pangolin scales stretched longitudinally (Long-Ori) at different strain rates, and the hydrated 100% relative humidity, dotted curves), showing significant decrease in strength and stiffness; (b) tensile stress-strain curves of Chinese pangolin scales stretched longitudinally (Long-Ori) at different strain rates, and the tensile behavior of the hydrated specimen (100% relative humidity, dotted curves); (c) strain rate sensitivities of African tree and Chinese pangolin scales, calculated via Eq. (2) with yield stresses obtained from (a) and (b); (d) strain rate sensitivities of human hair (keratinous material) and typical polymers (polycarbonate, PC, and polymethyl methacrylate (PMMA).

Another notable feature of keratinous materials is the hydration effect. The tensile stress-strain curves of hydrated (100% relative humidity) African tree and Chinese pangolin scales are overlaid in Fig. 12a and b (dotted curves), respectively. Both show significantly decreased Young's modulus and tensile strength but increased tensile strain (breaking strain not shown). The high hydration sensitivity is widely seen in other keratinous materials, e.g. human hair [50], stratum corneum [56], fingernails [6], feathers [50]. Based on extensive studies of α-keratin fibers, such humidity effect has been largely attributed to the interaction between water molecules and the amorphous matrix proteins, in which water may act cross link between chains, break down the secondary bonding and work as a plasticizer, thus reducing the stiffness and increasing the segmental mobility [6].

3.3.2.2. Fractography

Fig. 13 shows the tensile fracture surfaces of Chinese pangolin scales as strain rate increases from 10^{-5} to 10^{-3}, and to 10^{-1}/s. It is clear that they become smoother with increasing loading rate, and the fracture mode changes from fiber tear and fracture, lamella pull-out, to trans-lamellar fracture. At low strain rate (10^{-5}/s), lamellae are able to deform and delaminate into fibers (Fig. 13a), thus showing a rough fractured surface with torn fibers. A strain rate of 10^{-3}/s allows lamellae to move and shear, but not sufficiently to completely delaminate into fibers, thus exhibiting broken and pull-out lamellae with mesh-like surface (due to suture-like cell membrane complex). At relatively high strain rate (10^{-1}/s), lamellar movement is restricted, and lamellae are torn and fractured, displaying a smooth fracture surface with crossed-lamellae orientations. Such fracture mode change with increasing strain rate is also observed in hoof wall (α-keratin) [49] and bird beak rhamphotheca (β-keratin) [20,55]. The hoof wall shows highest degree of tubule pull-out fracture at lowest strain rate, and a more brittle surface fractured at impact. The crack propagation involves both parallel with and across the tubules depending on positions along the hoof wall thickness. As mentioned earlier, the bird beak rhamphotheca shows viscoplastic shear between scales (keratinized cells) at low strain rate and tensile fracture of the scales (keratinized cells) at high strain rate.

Pangolin scales show fracture surfaces of cracks following intercellular boundaries (between lamellae) at intermediate strain rates, and fracture surfaces indicating cracks through cells and interfaces (across lamellae) at lower and higher strain rates. This is similar to hoof wall that has a complex hierarchical structure featuring differentially oriented lamellae in tubules and intertubular materials [49]. The structural features of pangolin scales contribute to an enhanced toughening to resist fracture. The crossed-lamellae with fibers aligned in different orientations between layers make cracks propagate across lamellae more difficult, while the suture-like interfaces between lamellae increase the lamellar bonding, which requires more energy for delamination, and creates a tortuous crack path, dissipating more energy.

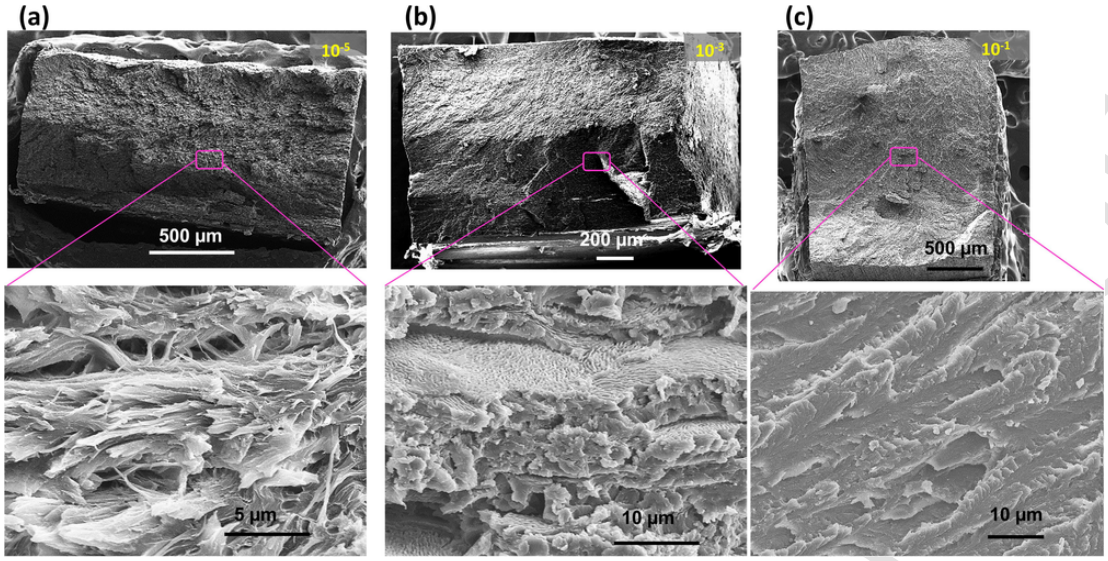

Fig. 13. Tensile fractured surfaces of the pangolin scale at (a) 10^{-5}/s, (b) 10^{-3}/s and (c) 10^{-1}/s. The fracture mode changes from fiber tear and fracture (lamellae delaminate into fibers) to lamella pull-out (lamella with surface suture) and trans-lamella fracture (smooth lamellar & cross-lamellar fracture) as strain rate increases.

4. Conclusions

The distinct structural features and mechanical properties of pangolin scales, a unique protection strategy for a mammal, are uncovered in the present work focused on understanding the design and protective functions. The following conclusions are drawn from characterization and testing:

- The overlap mechanism of both African tree (arboreal) and Chinese (ground) pangolin scales is that each scale sits in center of neighboring scales surrounding it in a hexagonal pattern; for each scale, the internal surface partially covers three lower scales, and the external surface is partially covered by upper three scales. The overlapping ratios on both the internal and external surfaces of Chinese and African tree pangolin scales are different due to the different shapes and dimensions.
- African tree and Chinese pangolin scales, composed of keratinized cells, show similar structure and mechanical properties. The scales have a cuticle structure composed of 3–5 layers of loosely attached keratinized cells with 40–70 μm in diameter and 0.5–1 μm in thickness. The interior structure consists of three regions: a dorsal region of flattened cells (diameter about ~30 μm and thickness 2–4 μm) forming crossed lamellae parallel to scale surface, a middle region of tilted and less flattened cells usually with larger dimensions (3–8 μm thick) constituting lamellae, and a ventral region that is similar to the dorsal region. At a still lower spatial scale, the nanostructure is comprised of filaments with 3–5 nm diameter. Each lamella is comprised of one layer of cells. Tensile deformation to failure reveals crossed fibers between lamellae. At the nanoscale, the scales show an interlocking interface between lamellae, which results from the suture-like cell membrane complex between keratinized cells.
- The tensile, compression and microindentation responses examined along different loading orientations reveal transverse isotropy in the plane of scale surface (E ~ 1 GPa; ultimate strength ~70 MPa at 10^{-3}/s) and a slightly higher strength along the scale thickness direction, correlating with the structure of crossed fibers and lamellae and keratinized cells.
- The keratin in the pangolin scales is strain-rate dependent, characteristic of a viscoelastic material, which become stiffer and stronger at fast loading to combat impacts (at 10^{-1}/s, the Young's modulus and tensile strength reach 1.5 GPa and 108.7 MPa, respectively), and are able to absorb large amount of energy when loaded at low strain rate (at 10^{-5}/s). The strain rate sensitivity values are 0.07 and 0.08 for African tree and Chinese pangolin scales, typical of polymers and hair keratin. The fracture mode changes from fiber tear and rupture, lamella pull-out, to trans-lamellar fracture with increasing strain rate, akin to a ductile-to-brittle transition. Hydration plays an important role in mechanical behavior, leading to significantly decreased Young's modulus (~0.27 GPa) and tensile strength (~34 MPa).

The structural features and the corresponding mechanical properties of pangolin scales are distinct from other typical keratinous materials, because of the specific functionalities required in the protection. The knowledge gained in this investigation will help advance our understanding of the biological solutions in designing materials and promote more efficient bioinspired structures.

Acknowledgement

The authors sincerely thank Scott Tremor, Mammalogist, at the San Diego Natural History Museum for providing pangolin scales for the current research. A special gratitude goes to Vincent R. Sherman and Chris Cassidy in the Mechanical and Aerospace Engineering Dept., UCSD, for helping us prepare tensile specimens using the laser machine. Vincent R. Sherman also helped preparing TEM specimens. We appreciate Shiteng Zhao at UCSD and Mason Mackey at the National Center for Microscopy and Imaging for providing help in TEM sample preparation and imaging. This work is supported by a China Scholarship Council for Postgraduate Students and an AFOSR MURI (AFOSR-FA9550-15-1-0009).

Appendix A. Supplementary data

Supplementary data associated with this article can be found, in the online version, at http://dx.doi.org/10.1016/j.actbio.2016.05.028.

References

[1] U.G.K. Wegst, M.F. Ashby, The mechanical efficiency of natural materials, Philos. Mag. 84 (21) (2004) 2167–2186.
[2] L.J. Gibson, M.F. Ashby, B.A. Harley, Cellular Materials in Nature and Medicine, Cambridge University Press, Cambridge, UK, 2010.
[3] M.A. Meyers, P.-Y. Chen, A.Y.-M. Lin, Y. Seki, Biological materials: structure and mechanical properties, Prog. Mater. Sci. 53 (1) (2008) 1–206.
[4] P.Y. Chen, J. McKittrick, M.A. Meyers, Biological materials: functional adaptations and bioinspired designs, Prog. Mater. Sci. 57 (8) (2012) 1492–1704.
[5] M.A. Meyers, J. McKittrick, P.-Y. Chen, Structural biological materials: critical mechanics-materials connections, Science 339 (6121) (2013) 773–779.
[6] B. Wang, W. Yang, J. McKittrick, M.A. Meyers, Keratin: structure, mechanical properties, occurrence in biological organisms, and efforts at bioinspiration, Prog. Mater. Sci. 76 (2016) 229–318.
[7] S.A. Wainwright, W.D. Biggs, J.D. Currey, J.M. Gosline, Mechanical Design in Organisms, Halsted Press, John Wiley & Sons, Inc., New York, 1976.
[8] M. Briggs, P. Briggs, The Encyclopedia of World Wildlife, Paragon Books, 2006.
[9] J. Kingdon, East African Mammals: An Atlas of Evolution in Africa, vol. I, University of Chicago Press, Chicago, 1974.
[10] M.E. Heath, Manis pentadactyla, The American Society of Mammalogist 414 (1992) 1–6.
[11] U. Rahm, Notes on pangolins of the ivory coast, J. Mammal. 37 (4) (1956) 531–537.
[12] W. Yang, I.H. Chen, B. Gludovatz, E.A. Zimmermann, R.O. Ritchie, M.A. Meyers, Natural flexible dermal armor, Adv. Mater. 25 (1) (2013) 31–48.
[13] R.I.C. Spearman, On the nature of the horny scales of the pangolin, J. Linn. Soc. Zool. 46 (310) (1967) 267–273.
[14] J. Tong, L.Q. Ren, B.C. Chen, Chemical constitution and abrasive wear behaviour of pangolin scales, J. Mater. Sci. Lett. 14 (20) (1995) 1468–1470.
[15] M. Feughelman, Mechanical Properties and Structure of Alpha-keratin Fibers: Wool, Human Hair and Related Fibers, University of New South Wales Press, 1997.
[16] L.J. Lynch, V. Robinson, C.A. Anderson, A scanning electron microscope study of the morphology of rhinoceros horn, Aust. J. Biol. Sci. 26 (2) (1973) 395–399.
[17] J.E. Bertram, J.M. Gosline, Fracture toughness design in horse hoof keratin, J. Exp. Biol. 125 (1986) 29–47.
[18] M. Feughelman, Keratin, second ed., Encyclopaedia of Polymer Science and Engineering, vol. 8, John Wiley and Son Inc, New York, , 1987566–600.
[19] M.A. Kasapi, J.M. Gosline, Design complexity and fracture control in the equine hoof wall, J. Exp. Biol. 200 (Pt 11) (1997) 1639–1659.
[20] Y. Seki, B. Kad, D. Benson, M.A. Meyers, The toucan beak: structure and mechanical response, Mater. Sci. Eng. C 26 (8) (2006) 1412–1420.
[21] J. Tong, Y.H. Ma, L.Q. Ren, J.Q. Li, Tribological characteristics of pangolin scales in dry sliding, J. Mater. Sci. Lett. 19 (7) (2000) 569–572.
[22] Z.Q. Liu, D. Jiao, Z.Y. Weng, Z.F. Zhang, Water-assisted self-healing and property recovery in a natural dermal armor of pangolin scales, J. Mech. Behav. Biomed. Mater. 56 (2016) 14–22.
[23] A. Jarrett, R.I. Spearman, J.A. Hardy, The histochemistry of keratinization, Br. J. Dermatol. 71 (1959) 277–295.
[24] B.K. Filshie, G.E. Gogers, An electron microscope study of the fine structure of feather keratin, J. Cell Biol. 13 (1) (1962) 1–12.
[25] D. Zhu, L. Szewciw, F. Vernerey, F. Barthelat, Puncture resistance of the scaled skin from striped bass: collective mechanisms and inspiration for new flexible armor designs, J. Mech. Behav. Biomed. Mater. 24 (2013) 30–40.
[26] D. Challender, J. Baillie, G. Ades, P. Kaspal, B. Chan, A. Khatiwada, L. Xu, S. Chin, R. KC, H. Nash, H. Hsieh, Manis pentadactyla, IUCN Red List of Threatened Species. Version 2014.2, 2014.
[27] S.E. Naleway, M.M. Porter, J. Mckittrick, M.A. Meyers, Structural design elements in biological materials: application to bioinspiration, Adv. Mater. 27 (37) (2015) 5455–5476.
[28] H. Ehrlich, Materials design principles of fish scales and armor, Biological Materials of Marine Origin, Springer, Netherlands, , 2014237–262.
[29] V.D. Burdak, Morphologie fonctionnelle du tegument ecailleux des poissons. Kiev: La Pensee Scientifique 1979 (in Russian). French translation, Cybium 10 (1986) 1–147.
[30] F.J. Meunier, J. Castanet, Organisation spatiale des fibres de collagene de la plaque basale des ecailles des Teleosteens, Zool. Scr. 11 (2) (1982) 141–153.
[31] D.G. Elliott, Chapter 5 – integumentary system (gross functional anatomy); Chapter 17 – integumentary system (microscopic functional anatomy), In: G.K. Ostrander (Ed.), The Laboratory Fish, Academic Press, Oxford, England, 2000. pp. 95–108, 271–306.
[32] W. Yang, B. Gludovatz, E.A. Zimmermann, H.A. Bale, R.O. Ritchie, M.A. Meyers, Structure and fracture resistance of alligator gar (Atractosteus spatula) armored fish scales, Acta Biomater. 9 (4) (2013) 5876–5889.
[33] A. Browning, C. Ortiz, M.C. Boyce, Mechanics of composite elasmoid fish scale assemblies and their bioinspired analogues, J. Mech. Behav. Biomed. Mater. 19 (2013) 75–86.
[34] W. Yang, C. Chao, J. McKittrick, Axial compression of a hollow cylinder filled with foam: a study of porcupine quills, Acta Biomater. 9 (2) (2013) 5297–5304.
[35] D.J. Tomlinson, C.H. Mülling, T.M. Fakler, Invited review: formation of keratins in the bovine claw: roles of hormones, minerals, and vitamins in functional claw integrity, J. Dairy Sci. 87 (4) (2004) 797–809.
[36] R.C. Marshall, D.F. Orwin, J.M. Gillespie, Structure and biochemistry of mammalian hard keratin, Electron Microsc. Rev. 4 (1) (1991) 47–83.
[37] G. Plewig, R.R. Marples, Regional differences of cell sizes in the human stratum corneum. Part I, J. Invest. Dermatol. 54 (1) (1970) 13–18.
[38] K.A. Holbrook, G.F. Odland, Regional differences in the thickness (cell layers) of the human stratum corneum: an ultrastructural analysis, J. Invest. Dermatol. 62 (4) (1974) 415–422.
[39] L. Tombolato, E.E. Novitskaya, P.Y. Chen, F.A. Sheppard, J. McKittrick, Microstructure, elastic properties and deformation mechanisms of horn keratin, Acta Biomater. 6 (2) (2010) 319–330.
[40] B.L. Lewis, Microscopic studies of fetal and mature nail and surrounding soft tissue, AMA Arch. Derm. Syphilol. 70 (1954) 733–747.
[41] H.P. Baden, The physical properties of nail, J. Invest. Dermatol. 55 (2) (1970) 115–122.
[42] L. Farran, A.R. Ennos, S.J. Eichhorn, The effect of humidity on the fracture properties of human fingernails, J. Exp. Biol. 211 (Pt 23) (2008) 3677–3681.
[43] T. Lingham-Soliar, N. Murugan, A new helical crossed-fibre structure of β-keratin in flight feathers and its biomechanical implications, PLoS ONE 8 (6) (2013).
[44] G.E. Rogers, Electron microscope studies of hair and wool, Ann. N.Y. Acad. Sci. 83 (3) (1959) 378–399.
[45] S. Krauss, E. Monsonego-Ornan, E. Zelzer, P. Fratzl, R. Shahar, Mechanical function of a complex three-dimensional suture joining the bony elements in the shell of the red-eared slider turtle, Adv. Mater. 21 (2009) 407–412.
[46] Y. Li, C. Ortiz, M.C. Boyce, Bioinspired, mechanical, deterministic fractal model for hierarchical suture joints, Phys. Rev. E Stat. Nonlinear Soft Matter Phys. 85 (3) (2012) 1–14.
[47] Y. Li, C. Ortiz, M.C. Boyce, A generalized mechanical model for suture interfaces of arbitrary geometry, J. Mech. Phys. Solids 61 (4) (2013) 1144–1167.
[48] W.E. Morton, J.W. Hearle, Physical Properties of Textile Fibres, third ed., The Textile Institute, Manchester, UK, 1993.
[49] M.A. Kasapi, J.M. Gosline, Strain-rate-dependent mechanical properties of the equine hoof wall, J. Exp. Biol. 199 (Pt 5) (1996) 1133–1146.
[50] B. Wang, M.A. Meyers, Unpublished results, 2016.
[51] E.W. Hart, Theory of the tensile test, Acta Metall. 15 (1967) 351–355.
[52] Y. Yu, B. Wang, M.A. Meyers, Unpublished results, 2015.
[53] G. Danilatos, M. Feughelman, Dynamic mechanical properties of α-keratin fibers during extension, J. Macromol. Sci. B 16 (4) (1979) 581–602.
[54] B.M. Chapman, 36 – The ageing of wool Part II: the ageing of disorganized fibres, J. Text. Inst. 66 (10) (1975) 343–346.
[55] Y. Seki, M.S. Schneider, M.A. Meyers, Structure and mechanical behavior of a toucan beak, Acta Mater. 53 (20) (2005) 5281–5296.
[56] K.S. Wu, W.W. Van Osdol, R.H. Dauskardt, Mechanical properties of human stratum corneum: effects of temperature, hydration, and chemical treatment, Biomaterials 27 (5) (2006) 785–795.